Small-Signal Analysis of Silicon Nanowire Transistors Based on a Poisson/Schrödinger/Boltzmann Solver

Maziar Noei*, Dino Ruić and Christoph Jungemann
Chair of Electromagnetic Theory
RWTH Aachen University
Aachen 52056, Germany
*Email: mn@ithe.rwth-aachen.de

***Abstract*—A small-signal solver for junctionless nanowire field-effect transistors, capable of doing exact simulations in the full frequency range is presented for the first time. The solver uses a deterministic framework and shows great stability due to the transformation from kinetic energy to total energy and even/odd splitting of the distribution function. Small-signal terminal currents are calculated using the Ramo-Shockley theorem, and the simulation results are shown to satisfy the necessary conditions such as being reciprocal and passive in equilibrium.**

I. Introduction

With the 10nm technology generation being under intensive development, the change in geometry of field-effect transistors from fin to wire is expected to further enable device scaling due to better short-channel control as well as high current density [1], [2]. Since working in short-channel regimes and introducing such spatial confinements inevitably leads to more pronounced quantum mechanical effects, numerical investigation of these nanowire transistors requires approaches beyond the classical drift-diffusion and hydrodynamic models [3]. On the other hand, fully quantum-mechanical approaches such as the density-functional theory and the non-equilibrium Green's function (NEGF) formalism [4] are not suitable for simulation of devices with decananometer channel lengths due to their huge computational costs.

In this regard, semi-classical simulators based on Boltzmann's equation (BE) have become increasingly popular, with the usual approach being to self-consistently solve the coupled system of Poisson, Schrödinger, and Boltzmann equations in Gummel-type iterations [5], [6]. Their deterministic nature allows us to easily simulate rare events, deep-subthreshold operating points, and events on completely different time scales; an important feature that stochastic Monte Carlo simulators lack. In [7], we presented for the first time a quadratically converging stable full Newton-Raphson (FNR) nanowire transistor solver for the combined system of Poisson, Schrödinger and Boltzmann equations, which was shown to be superior to the previously presented Gummel-type iteration schemes both in convergence behavior and in total solver time. The main advantage of such FNR approach, however, becomes evident when we notice how such formulation can pave the way towards exact small-signal analysis, i.e. once an FNR solver is available for the stationary problem, our system of equations is already linearized and the same derivatives can be used in investigation of small AC perturbations covering the full frequency range.

Hence, the first small-signal investigation of silicon nanowire transistors based on the multi-subband determinisitc framework in [7] is presented in this work. The paper is organized as follows: In Section II, we briefly explain the details of our solver and go over the techniques used for achieving stability and precision while maintaining a relatively low computational cost. In Section III, the small-signal solver is validated by presenting and discussing the numerical results of simulations. Using the obtained small-signal parameters, device stability can be evaluated because stability factors (e.g., Rollets stability factor) can be easily determined. Similarly, the ultimate limits of the device in gain and frequency figures of merit (such as short-circuit current gain and cut-off frequency) will be presented and discussed. Conclusions are finally given in Section IV.

II. Model

Fig. 1 shows a schematic cross-sectional view of the junctionless silicon nanowire transistor under study. The z direction is the transport (longitudinal) direction and x, y the transverse directions.

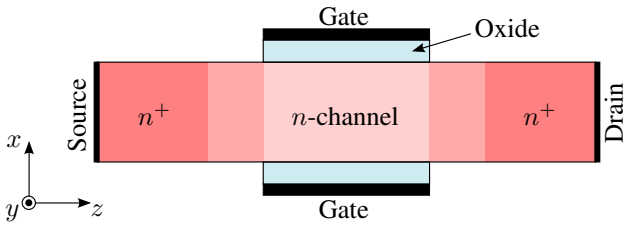

Fig. 1. Two-dimensional cross sectional view of a gate-all-around junctionless nanowire transistor along the transport direction. The oxide (assumed to be SiO_2 in this work) thickness is $t_{ox} = 1$nm.

A. Steady-State Analysis

The Poisson equation is solved for the electrostatic potential in the 3D real space. The finite volume method is used to ensure flux conservation in the discretization process. In order to treat strong quantization effects, the time-independent Schrödinger equation (SE) is numerically solved in $x-y$ slices perpendicular to the transport direction using the FEAST eigensolver package [8].

The 1D Boltzmann transport equation is discretized using H-transformation [9], [10], which removes the derivative with respect to k_z and aligns the energy grid with the trajectories of ballistic carriers. Splitting the electron distribution function into its even and odd parts on a staggered grid [10] followed by an odd-elimination step in our system of equations, results in the discretized free-streaming term being unconditionally stable. Regarding the scattering term, different inter-valley and intra-valley electron-phonon interactions are included in our solver [11].

The coupled Boltzmann, Poisson, and Schrödinger equations are solved by the Newton-Raphson scheme, with the unknown variables being the electrostatic potential $\varphi(\mathbf{r})$ and the distribution function $f^{\nu}(z,H)$ [7]. $\nu=(v,s)$ captures both the valley index and the subband index. Since the Schrödinger equation, being an eigenvalue problem, cannot be directly cast into the Newton-Raphson matrix equation, the first order time-independent perturbation theory is used to express the changes in subband energies and wavefunctions in terms of changes in $\varphi(\mathbf{r})$ and calculate the corresponding derivatives [12]. In order to avoid divergence in the first iterations, we start the simulation with Gummel-type iterations up to a predefined threshold and then switch to the Newton-Raphson solver.

B. Small-signal Analysis

Since the small-signal analysis requires linearization of the system of equations around the stationary values, its matrix equation is closely related to Newton-Raphson equations, i.e. apart from the time-derivative in BE, all of the coefficients are already available since we have constructed the Jacobian matrix for our Newton-Raphson system earlier. Since the small-signal computations are often performed for many frequencies, the steady-state solutions and the corresponding Jacobian matrix are saved after the convergence of Newton-Raphson system and reused at each frequency value. Hence, the time-consuming evaluation of the Jacobian matrix is avoided. However, carelessly moving from the continuous BE to the discretized one might lead to unexpected problems with the reciprocity and passivity of the small-signal parameters in equilibrium conditions. Factorization of the distribution function into its equilibrium and non-equilibrium parts as explained in [13], and making sure that we have a consistent formulation of BE and PE in small-signal sense, restores the necessary symmetries.

The small-signal terminal currents are calculated using a formulation of the Ramo-Shockley theorem that is consistent with the simulation framework, i.e. one-dimensional BE along the transport direction and two-dimensional SE in the transverse planes [14].

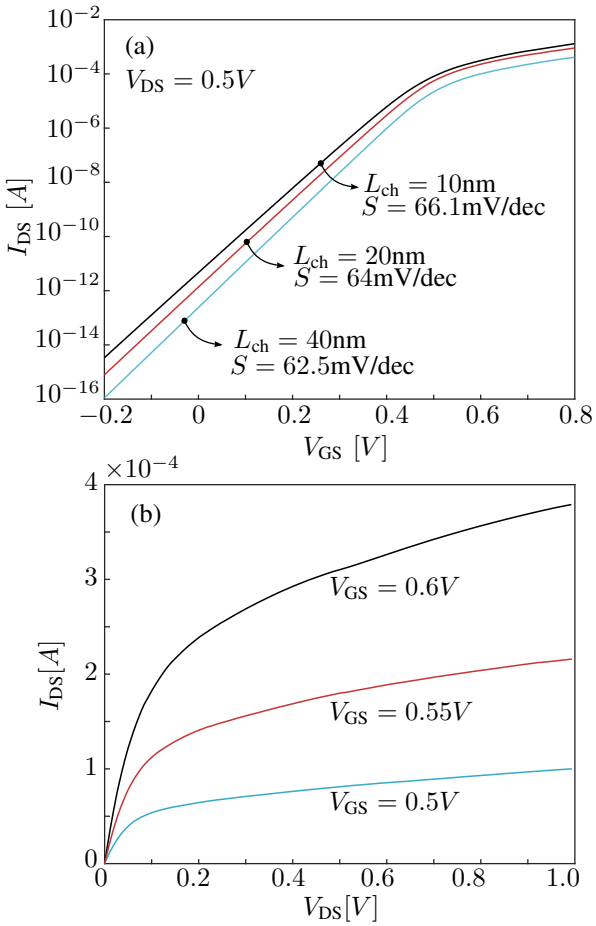

Fig. 2. (a) Calculated $I_{\mathrm{DS}}-V_{\mathrm{GS}}$ characteristics of the simulated device for different channel lengths, (b) $I_{\mathrm{DS}}-V_{\mathrm{DS}}$ output characteristics at different gate biases.

III. Results

For the following simulations, we have extended an irregular 2D Delauney grid in the $x-y$ plane non-equidistantly in the transport direction. This non-equidistant grid construction allows us to have a better resolution near the large potential gradients while being able to extend the n^{+}-regions without adding much to the computational cost. The source/drain regions are 60nm long each, with doping concentration of $N_{\mathrm{D}}^{+}=2\times10^{19}\mathrm{cm}^{-3}$. The channel region is doped to $N_{\mathrm{D}}=1\times10^{17}\mathrm{cm}^{-3}$, and $L_{\mathrm{ch}}=L_{\mathrm{G}}$ is assumed. In order to correctly calculate the first-order perturbations in constructing the Newton-Raphson system, we need to solve the SE for all of the subbands. However, for a nanowire cross-section of 5nm×4nm, we can safely limit ourselves to the 5 lowest subbands in the BE. Regarding the H-grid, a grid spacing of $\Delta H=5.24\mathrm{meV}$ is chosen.

First, we demonstrate the results for steady-state simulations. Fig. 2(a) and Fig. 2(b) show the transfer characteristics of the simulated device at $V_{\mathrm{DS}}=0.5V$ for three different channel lengths and the $I_{\mathrm{DS}}-V_{\mathrm{DS}}$ output characteristics for

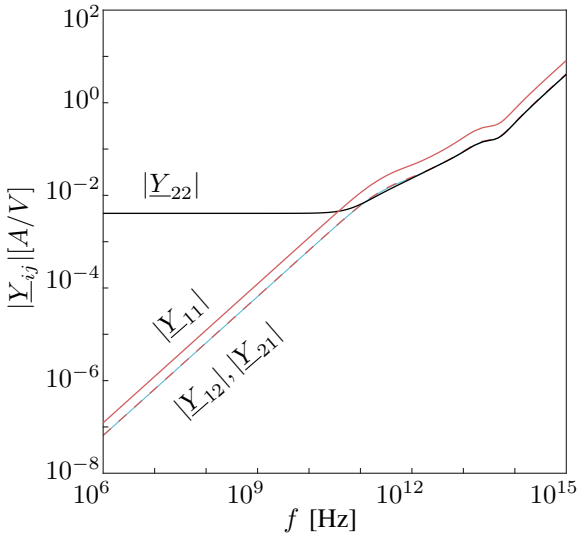

Fig. 3. Absolute value of admittance parameters vs. frequency at $V_{\mathrm{GS}} = 0.5V$ and $V_{\mathrm{DS}} = 0V$. $|\underline{Y}_{12}|$ and $|\underline{Y}_{21}|$ are equal to the precision of 10^{-14}, and cannot be distinguished from each other in the figure.

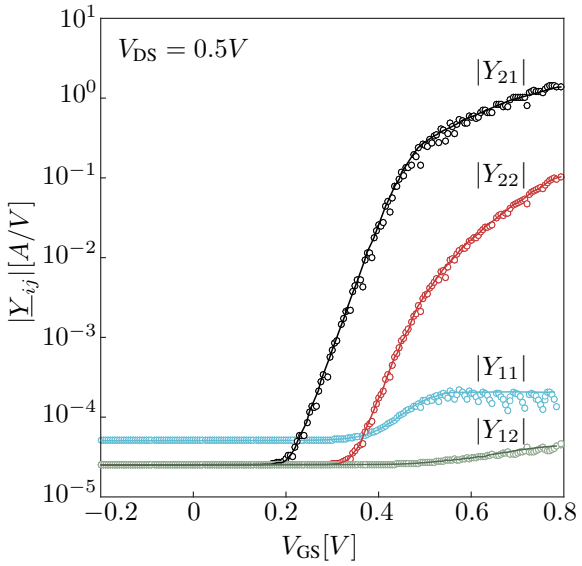

Fig. 4. Absolute value of admittance parameters vs. gate bias at $f = 10GHz$.

different V_{GS} values, respectively. Our solver shows great stability and easily produces very smooth DC curves which span more than 10 decades of magnitude. Such deep-subthreshold simulations are practically impossible with non-deterministic Monte Carlo methods.

Figure 3 shows the admittance parameters versus frequency at $V_{\mathrm{GS}} = 0.5V$ and $V_{\mathrm{DS}} = 0V$, i.e. in equilibrium. For a non-magnetized two-port, $\underline{Y}_{12} = \underline{Y}_{21}$ must hold in equilibrium conditions (the reciprocity requirement), and the figure shows that this is surely satisfied in our discretized description.

The admittance parameters versus the gate bias for $V_{\mathrm{DS}} = 0.5V$ are shown in Fig. 4. The simulation results show discontinuities, which are artifacts of discretization in H-space. Whenever a subband moves continuously from one energy box to another, discontinuities in the derivatives with respect to electrostatic potential occur. As a result, these kinds of discontinuities appear whenever some small-signal parameter is plotted against a contact bias (having H-transformation utilized in the discretization process). In fact, the stationary quantities such as the steady-state currents shown in Fig. 2 also exhibit discontinuities in their derivatives with respect to contact biases. But these changes are completely negligible on scales of interest. Small-signal parameter, on the other hand, are strongly influenced by the details of discretization schemes, the impact of which could be made arbitrarily small by refining the energy grid.

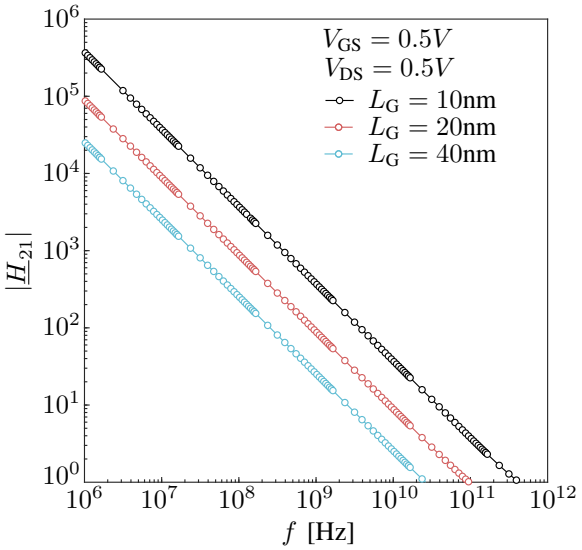

Fig. 5. Small-signal current gain $|\underline{H}_{21}|$ versus frequency for different channel lengths.

The small-signal current gain $|\underline{H}_{21}| = |\underline{Y}_{21}/\underline{Y}_{11}|$ is extracted from the admittance parameters and plotted against frequency in Fig. 5 for different channel lengths. Deviations

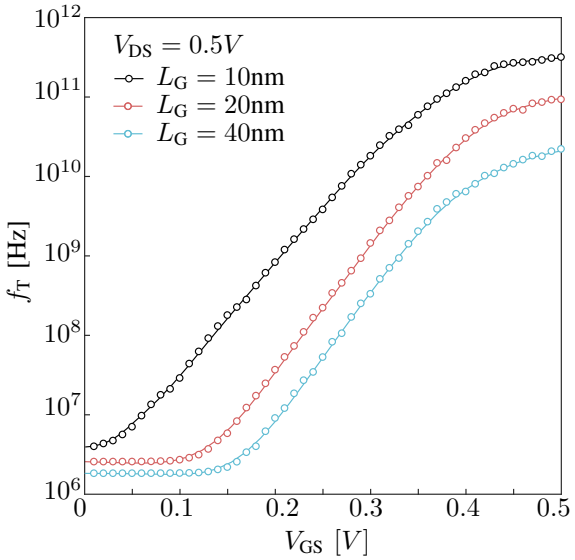

Fig. 6. Cut-off frequency as a function of V_{GS} for different channel lengths.

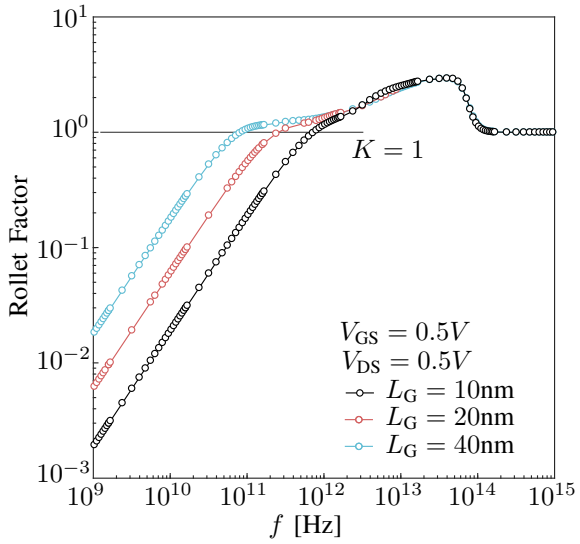

Fig. 7. Rollet's stability factor versus frequency for different channel lengths.

of $|H_{21}(f)|$ from the typical $1/f$ dependency are negligible, and the obtained f_{T} values for $L_G = 10$nm, 20nm, and 40nm are $f_{\mathrm{T}} = 398$GHz, 95.9GHz, and 23.8GHz, respectively. Next, the cut-off frequencies for these gate lengths are calculated at different V_{GS} values. The results, shown in Fig. 6, show discontinuities rather similar to those observed in Fig. 4.

Fig. 7 demonstrates the stability factor defined as,

$$K = \frac{2\Re\{\underline{Y}_{11}\}\Re\{\underline{Y}_{22}\} - \Re\{\underline{Y}_{12}\underline{Y}_{21}\}}{|\underline{Y}_{12}\underline{Y}_{21}|} \qquad (1)$$

for different gate length values. Since $\Re\{\underline{Y}_{11}\}$ and $\Re\{\underline{Y}_{22}\}$ are positive in the simulated frequency range, the device would be unconditionally stable at frequencies in which $K > 1$. The critical frequency (f_{k}, defined as the frequency above which the device is unconditionally stable) for the transistors with L_{G} =10, 20 and 40nm were about 740GHz, 276GHz, and 91GHz at $V_{\mathrm{GS}} = V_{\mathrm{DS}} = 0.5V$, respectively. Consequently, the additional stability circuits are not required for RF circuits above these frequencies. The reduction in gate length leads to increase in short-channel effect and has the impact on stability performance.

IV. Conclusion

In this work, a semi-classical deterministic nanowire solver suitable for small-signal simulations was presented. The simulation framework allows for robust and stable computations in the complete frequency range and for a wide range of bias conditions. The small-signal solver was validated by presenting and discussing the numerical results of simulations. The calculated small-signal parameters show reciprocity and passivity in equilibrium conditions, and are perfectly smooth when plotted against frequency. However, they change discontinuously by continuously changing any quantity that influences the steady-state potential within the device. These minor and negligible discontinuities are direct consequences of transforming the BE into total energy, and can be made arbitrarily small by refining the energy grid. Since small-signal analysis is a vital component of modern device simulations, the presented solver can be of great use in investigation and prediction of nanowire devices for RF and high-frequency applications.

References

[1] S. R. Mehrotra, K. SungGeun, T. Kubis, M. Povolotskyi, M. S. Lundstrom, and G. Klimeck, "Engineering nanowire n-MOSFETs at $L_{\mathrm{G}} < 8$nm," *Electron Devices, IEEE Transactions on*, vol. 60, pp. 2171–2177, 2013.

[2] S. D. Kim, M. Guillorn, I. Lauer, P. Oldiges, T. Hook, and M. H. Na, "Performance trade-offs in FinFET and gate-all-around device architectures for 7nm-node and beyond," *2015 IEEE SOI-3D-Subthreshold Microelectronics Technology Unified Conference (S3S)*, pp. 1–3, 2015.

[3] C. Jungemann, T. Grasser, B. Neinhüs, and B. Meinerzhagen, "Failure of moments-based transport models in nanoscale devices near equilibrium," *Electron Devices, IEEE Transactions on*, vol. 52, no. 11, pp. 2404–2408, 2005.

[4] M. Chakraverty, H. PS, and V. Ruparelia, "Effect of scaling of device parameters on the performance of uncoupled mode space NEGF transport model based silicon nanowire transistor," *2016 International Conference on Energy Efficient Technologies for Sustainability (ICEETS)*, pp. 746–755, 2016.

[5] S. Jin, M. V. Fischetti, and T. w. Tang, "Theoretical study of carrier transport in silicon nanowire transistors based on the multisubband Boltzmann transport equation," *Electron Devices, IEEE Transactions on*, vol. 55, pp. 2886–2897, 2008.

[6] S. Scaldaferri, G. Curatola, and G. Iannaccone, "Direct solution of the boltzmann transport equation and poisson/schrödinger equation for nanoscale mosfets," vol. 54, no. 11, 2007.

[7] M. Noei and C. Jungemann, "Numerical investigation of junctionless nanowire transistors using a boltzmann/schrdinger/poisson full newton-raphson solver," *Proc. SISPAD*, 2016.

[8] E. Polizzi, "Density-matrix-based algorithm for solving eigenvalue problems," *Phys. Rev. B*, vol. 79, p. 115112, Mar 2009.

[9] A. Gnudi, D. Ventura, G. Baccarani, and F. Odeh, "Two-dimensional MOSFET simulation by means of a multidimensional spherical harmonics expansion of the Boltzmann transport equation," *Solid–State Electron.*, vol. 36, no. 4, pp. 575 – 581, 1993.

[10] S.-M. Hong, A. T. Pham, and C. Jungemann, *Deterministic solvers for the Boltzmann transport equation*. Computational Microelectronics, Wien, New York: Springer, 2011.

[11] D. Esseni, P. Palestri, and L. Selmi, *Nanoscale MOS Transistors. Semi-Classical Transport and Applications*. Cambridge University Press, 2011.

[12] R. Shankar, *Principles of quantum mechanics*. New York: Springer, 1994.

[13] D. Ruić and C. Jungemann, "Numerical aspects of noise simulation in MOSFETs by a Langevin-Boltzmann solver," *Journal of Computational Electronics*, vol. 14, no. 1, pp. 21–36, 2015.

[14] H. Kim, H. S. Min, T. W. Tang, and Y. J. Park, "An extended proof of the Ramo-Shockley theorem," *Solid–State Electron.*, vol. 34, pp. 1251–1253, 1991.